

Parameterization of the Woods-Saxon Potential for Shell-Model Calculations

N.Schwierz,* I. Wiedenhöver, and A. Volya

Florida State University, Physics Department, Tallahassee, FL 32306

(Dated: February 11, 2013)

The drastically expanded use of the Woods-Saxon potential in modern day nuclear physics and the availability of new nuclear data motivated us to review and optimize the parameters of this potential to the experimental single-nucleon spectra around the doubly-magic nuclei between ^{16}O and ^{208}Pb . We obtain a parameterization which is applicable over the whole nuclear chart for nuclides between ^{16}O and the heaviest elements. Apart from Coulomb components the obtained parameter set is isospin symmetric. We demonstrate that the potential provides a good description of the nuclear mean field leading to quality single-particle spectra, nuclear radii, prediction of drip-lines, shell closures and other properties. This presented Woods-Saxon fit provides an adequate single-particle basis for shell model calculations bridging over into the continuum.

PACS numbers: 21.19.-k, 21.60.-n

I. INTRODUCTION

The description of the nuclear many-body system by an effective mean field is a doorway to the understanding of atomic nuclei. The averaged single nucleon dynamics in the field of all other nucleons is a starting point in practically all many-body methods. In this context, a good choice of single-nucleon basis states is the key for success in any quantum many-body approach. A plethora of experimental observations such as magic numbers, shell gaps, binding energies, nuclear radii, abundances of nuclei in nature and reaction properties all confirm the remarkable success of the very simple, pure mean field picture.

Generally, the motion of non-interacting particles in the mean field is not an exact solution to the many-body problem. Residual interactions or collective dynamics of the mean field itself are present. The Hartree-Fock or Hartree-Fock-Bogoliubov approach allows to variationally find the best possible mean field thus minimizing the residual interactions. The technique has been demonstrated to be very successful. Nevertheless, at present it is still a challenge to find the best mean field with properly preserved symmetries, not to mention the interactions and related physics that go beyond the Hartree-Fock approach.

In contrast, in a very simple approach the mean field can be taken in the form of a three dimensional harmonic oscillator, which provides an analytical set of basis states. The possibility of an exact translationally invariant treatment with full center of mass extraction is particularly appealing. Historically, the harmonic oscillator mean field with added spin orbit term was the first successful mean field treatment, by which the correct sequence of orbitals and the magic numbers was predicted [1].

In order to achieve a quantitative description of nuclei, oscillator parameters have to be selected in dependence of the nuclear mass. Typically, for spherical nuclei of mass A , the oscillator parameter $\hbar\omega = 41/A^{1/3}$ MeV provides a good description, which was found by comparing the oscillator rms mass radius with experiment. The analytical form of the single particle basis comes at the expense of relatively strong residual particle-particle interactions. Still, very successful shell-model descriptions have been developed on the basis of the harmonic oscillator [2], where the many-body Hamiltonian that includes residual interactions is diagonalized exactly.

Present day nuclear physics has expanded its reach far beyond the valley of stability into regions of the nuclear chart where the continuum spectrum of the mean field potential becomes important. To address these situations or for the purposes of nuclear reaction physics, the choice of a Woods-Saxon [3] potential as a model for the mean field has become a common approach. The analyticity of solution in the harmonic oscillator is traded for the presence of a continuum spectrum and a potential resembling the geometric distribution of nuclear density. Although the single particle states must be found numerically, such computations are trivial with today's computers, making the numerical approach preferential over analytically solvable models such as Ginocchio potential [4] or the square well. Other forms of potentials have been considered in the past [5]. With little exception, all modern theoretical techniques dealing with the physics on the interface of structure and reactions have their roots in the Woods-Saxon potential [6, 7].

A number of parameterizations of the Woods-Saxon potential have been published, created with different objectives and relevant to different nuclear mass regions. Most commonly used is the so-called "Universal" parameterization [8], which was adjusted to reproduce the single-particle binding energies of proton and neutron orbitals around the doubly-magic nucleus ^{208}Pb and correct ground state spins for nuclei of masses around $A=180$, but claimed to be applicable to lighter mass regions as well. Characteristic for the "Universal" parameterization

*Also at Physics Department, Universität Konstanz, Konstanz, Germany

is the choice of different radii for the proton- and neutron potentials. It has been pointed out, that this parameterization has shortcomings with respect to lighter nuclei and that it predicts charge radii inconsistent with experiment. [9].

The importance of a good starting parameterization of the mean field potential, its expanded use in the context of the continuum shell model and the availability of new experimental data motivated us to revisit the question of parameters in the Woods-Saxon potential. In this work we find a set of parameters to be considered as a global Woods-Saxon parameterization, obeying the symmetry principles of isospin conservation in the nuclear interaction as well as correct two-body kinematics. We use a set of single particle and single hole states in the vicinity of doubly-magic nuclei ^{16}O , ^{40}Ca , ^{48}Ca , ^{56}Ni , ^{100}Sn , ^{132}Sn and ^{208}Pb to provide experimental input on the single particle data. We adjust the potential parameters to reproduce the experimental data by applying a least-squares fit algorithm.

This work is a continuation and extension of a previous effort to determine a globally applicable set of Woods-Saxon potential parameters. Among the similarities between our work and the previous parameter set is the isospin-symmetry of the nuclear potential. While the previously obtained parameter set was not published, a total-Routhian-surface calculation based on it was discussed in [10].

The paper is organized as follows. In section II, we describe the experimental data that is used in optimizing the parameters, in section III we address the properties of the Woods-Saxon Hamiltonian, its symmetries and the parameterization. In section IV we describe the calculation of the orbitals of the Woods-Saxon potential and the least squares fit algorithm employed to adjust the parameters to fit the experimental data. The predictions of our Woods-Saxon potential for rms charge radii and neutron radii is discussed in section V, as well as its predictions for certain neutron-rich nuclides.

II. SINGLE PARTICLE LEVEL DATA

Basis for this investigation are the experimental single particle spectra around the doubly magic nuclei ^{16}O , ^{40}Ca , ^{48}Ca , ^{56}Ni , ^{132}Sn and ^{208}Pb . These systems were chosen, because they are expected to show the most pure experimental manifestation of single-particle excitations. The binding energies of the single-nucleon orbitals around a magic nucleus of mass A were extracted from the excited states of the neighboring nuclei by

$$\epsilon(A, I^\pi) = \Delta M(A) - (\Delta M(A-1) + \Delta M(1)) - E(I^\pi) \quad (1)$$

for hole-states,

$$\epsilon(A+1, I^\pi) = \Delta M(A+1) - (\Delta M(A) + \Delta M(1)) + E(I^\pi) \quad (2)$$

1d _{3/2} neutron ^{17}O				1d _{3/2} proton ^{17}F			
Ex	E _{ν}	Γ_n [keV]	S^a	Ex	E _{π}	Γ_p [keV]	S^b
5.085	0.937	96	0.689	5.000	4.400	1530	0.845
5.869	1.721	6.6	0.010	5.820	5.220	180	0.057
7.202	3.052	280	0.169	7.479	6.879	795	0.097
8.070	3.916	71	0.085	8.760	8.160	90 ^c	0.000
8.897	4.751	68	0.042				
5.836	1.710		0.995	5.288	4.688		1.000

Table I: $d_{3/2}$ resonances in ^{17}O and ^{17}F , energies are in MeV. The bottom line corresponds to the adopted weighted single particle energies.

^aThe spectroscopic factors are from R-matrix analysis in Ref. [23]

^bOur parametrization with adjusted potential depth was used to compute the single particle decay width at the experimental energies, the ratio of experimental width to single particle determined the spectroscopic factor S . The total strength was normalized to 1.

^cThe proton channel is only 20% of the total width.

for particle-states. Here $\Delta M(A)$ denotes the experimental mass defects of a nucleus with mass number A and $E(I^\pi)$ the excitation energy of a given state. Both proton and neutron orbitals are considered.

The experimental data were generally extracted from the NNDC data base [11] - [22], selecting data sets representing single-proton or neutron transfer or pickup reactions, where available. For the ^{40}Ca , ^{48}Ca and ^{208}Pb nuclides, some of the single-particle and single-hole strength was observed to be fragmented over a number of individual states. In these cases, we calculate the orbital energy from an average excitation energy of the states, weighted with the single-particle spectroscopic factors. The cases for which the data base showed contradictory experimental results are discussed separately in the following paragraphs. The data set of orbital energies used in this study and the relevant experimental information is summarized in the Table II.

In the case of ^{17}F and ^{17}O , we used $d_{5/2}$ and $s_{1/2}$ states established by direct transfer-reactions. However, the corresponding $d_{3/2}$ orbits are unbound and their strength is fragmented over a number of resonances, both in ^{17}F and ^{17}O . The resonance data for neutron scattering on ^{16}O was taken from Ref. [23], including the analysis of spectroscopic factors. The analogous factors for protons were extracted from the ratio of the observed proton-resonance widths [12] to a single-particle decay width calculated with our Woods-Saxon potential for the experimental kinematics. The results are summarized in Tab. I.

For the case of proton orbitals in ^{40}Ca , the Nuclear Data Sheets entry for ^{39}K [13] shows a state at 8.43 MeV excitation energy, which is assigned $d_{3/2}$ character with a spectroscopic factor of $C^2S=0.24$, based on data published in Ref. [24]. We excluded this state from our analysis, for two reasons; First it would represent a rather unusual fragmentation of single-particle strength, placing

a fragment of the ground state at over 8 MeV excitation energy. Second, including it would lead to inconsistent Coulomb shifts between the proton and neutron orbitals. The assignment of $d_{3/2}$ in Ref. [24] was based on an angular distribution measurement, but the difference between a $d_{3/2}$ assignment and the more likely $d_{5/2}$ assignment seems inconclusive from the data presented in the publication. In view of this assessment, we based our analysis of the ^{39}K data on the older measurement of [25]. Note that, after excluding the above mentioned $d_{3/2}$ assignment, the data from both references [25] and [24] leads to almost identical energies of s.p. orbitals.

For ^{56}Ni , only one experiment for a direct neutron-transfer is published, based on the (d, p) reaction [27]. This experiment revealed spectroscopic factors of single-particle character for the lowest $3/2^-$, $5/2^-$ and $1/2^-$ states. For the proton orbitals, no direct spectroscopic factor measurements are available to date, however, the lowest $3/2^-$, $5/2^-$ and $1/2^-$ states show consistent Coulomb-shifts, and therefore were assumed to be the analog proton excitations.

^{100}Sn is still beyond the reach of today's radioactive beam facilities, but systematic studies of the shell structure of nuclides approaching it have produced a set of effective single particle orbitals[30], which we include in our investigation.

For the doubly-magic nucleus ^{132}Sn no single-particle reactions were published to date. However, the level schemes of nuclei around ^{132}Sn are well established from β -decay measurements. Using data from the NNDC data base [19, 20], we identified the lowest states of given spin and parity with the single-particle or single hole states of the orbitals in question, and experimental binding energies for the ground states.

^{208}Pb has been studied by a multitude of experiments. The spectrum of single-particle and hole excitations seems well established by the measured large spectroscopic factors [21, 22]. Nevertheless, even for this textbook doubly magic nucleus, some fragmentation of the orbital strengths can be expected for high excitation energies. Data on the fragmentation of proton and neutron hole states around ^{208}Pb was established in Refs. [28] and [29]. Although these experiments show the main orbital strength to be concentrated in one state for each orbital, the smaller fragments lead to significant centroid energy shifts, approximately 0.5 MeV for the deepest hole states. In contrast to this situation, no data on the fragmentation for the neutron and proton particle states was found in the literature, in spite of the large number of published experimental studies. It seems worth while to revisit experiments on the fragmentation of single particle structure around ^{208}Pb with modern experimental techniques in order to address this apparent deficiency of the experimental data.

Table II: Systematics of nuclear single particle energies. In the first three columns, we list the orbital type, extracted binding energy, and excitation energy of the single particle level. The binding and excitation energies are weighted with spectroscopic factors (see text), the value of the total spectroscopic strength $\mathcal{S} = \sum S = \sum C^2 S / (2j + 1)$ appears in the fourth column for the cases where relevant experimental information is available. The fifth column identifies individual excited states used in the analysis.

Orbital	Energy [MeV]	E_x [MeV]	\mathcal{S}	individual states [MeV]
^{16}O				
neutron hole				^{15}O [11]
$1p_{1/2}$	-15.66	0		0
neutron particle				^{17}O [23]
$1d_{5/2}$	-4.14	0	1.00	0
$2s_{1/2}$	-3.27	0.87	1.00	0.87
$1d_{3/2}$	1.710	5.836	1.00	see Tab. I
proton hole				^{15}N [11]
$1p_{1/2}$	-12.13	0	1.13	0
proton particle				^{17}F [12]
$1d_{5/2}$	-0.60	0	0.94	0
$2s_{1/2}$	-0.11	0.495	0.83	0.495
$1d_{3/2}$	4.688	5.288	1.00	see Tab. I
^{40}Ca				
neutron hole				^{39}Ca [25]
$1d_{5/2}$	-22.39	6.744	0.90	21 states between 4.320 and 9.500 MeV
$2s_{1/2}$	-18.19	2.533	0.82	2.463, 4.017
$1d_{3/2}$	-15.64	0	0.94	0
neutron particle				^{41}Ca [26]
$1f_{7/2}$	-8.36	0	0.77	0
$2p_{3/2}$	-5.84	2.519	0.91	1.940, 2.461, 3.731, 4.602
$2p_{1/2}$	-4.20	4.157	0.70	3.613, 3.943, 4.109, 4.754
$1f_{5/2}$	-1.56	6.801	0.95	24 states between 4.878 and 9.084
proton hole				^{39}K [25]
$1d_{5/2}$	-15.07	6.738	0.83	16 states between 5.262 and 9.750
$2s_{1/2}$	-10.92	2.593	0.87	2.520, 4.095
$1d_{3/2}$	-8.33	0	0.93	0
proton particle				^{41}Sc [14]
$1f_{7/2}$	-1.09	0	1.12	0
$2p_{3/2}$	0.69	1.784	0.94	1.716, 2.419
$2p_{1/2}$	2.38	3.471	0.75	3.471
$1f_{5/2}$	4.96	5.685	0.33	5.709, 3.192, 5.862, 6.470
^{48}Ca				
neutron hole				^{47}Ca [15]
$1d_{5/2}$	-15.61	5.669	0.15	4.980, 5.300, 5.450, 6.250, 6.870
$2s_{1/2}$	-12.55	2.600	0.90	2.600
$1d_{3/2}$	-12.53	2.580	0.90	2.580
$1f_{7/2}$	-10.00	0.050	0.85	0, 3.300, 3.430
neutron particle				^{49}Ca [16]
$2p_{3/2}$	-4.60	0.545	0.97	0, 4.069
$2p_{1/2}$	-2.86	2.282	1.03	2.021, 4.261
$1f_{5/2}$	-1.20	3.946	0.95	3.586, 3.993
$1g_{9/2}$	0.130	5.276	0.47	4.018, 4.887, 5.378, 6.529, 6.753
proton hole				^{47}K [15]

Table II – Continued

Orbital	Energy [MeV]	E_x [MeV]	S	individual states [MeV]
$1d_{5/2}$	-21.47	5.664	0.62	3.432, 5.220, 5.465, 6.462, 7.740, 8.020, 8.530
$1d_{3/2}$	-16.18	0.377	1.22	0.359, 3.930
$2s_{1/2}$	-16.10	0.295	0.92	0, 3.850
proton particle				^{49}Sc [16]
$1f_{7/2}$	-9.35	0.278	0.91	0, 3.809
$2p_{3/2}$	-6.44	3.187	0.54	3.085, 6.717
$2p_{1/2}$	-4.64	4.984	0.88	4.495, 5.015, 5.663, 6.816
^{56}Ni				
neutron hole				^{55}Ni [17]
$1f_{7/2}$	-16.64	0		0
neutron particle				^{57}Ni [27]
$2p_{3/2}$	-10.25	0	0.91	0
$1f_{5/2}$	-9.48	0.768	0.91	0.768
$2p_{1/2}$	-9.13	1.113	0.90	1.113
proton hole				^{55}Co [17]
$1f_{7/2}$	-7.17	0		0
proton particle				^{57}Cu [18]
$2p_{3/2}$	-0.69	0		0
$1f_{5/2}$	0.33	1.028		1.028
$2p_{1/2}$	0.41	1.106		1.106
^{100}Sn [30], see note ^a				
neutrons				
$2p_{1/2}$	-18.38(20)			
$1g_{9/2}$	-17.93(30)			
$2d_{5/2}$	-11.13(20)			
$1g_{7/2}$	-10.93(20)			
$3s_{1/2}$	-9.3(5)			
$1h_{11/2}$	-8.6(5)			
$2d_{3/2}$	-9.2(5)			
protons				
$1f_{5/2}$	-8.71			
$2p_{3/2}$	-6.38			
$2p_{1/2}$	-3.53(20)			
$1g_{9/2}$	-2.92(20)			
$2d_{5/2}$	3.00(80)			
$1g_{7/2}$	3.90(15)			

Table II – Continued

Orbital	Energy [MeV]	E_x [MeV]	S	individual states [MeV]
^{132}Sn , see note ^b				
neutron hole				^{131}Sn [19]
$1g_{7/2}$	-9.75	2.434		2.434
$2d_{5/2}$	-8.97	1.655		1.655
$3s_{1/2}$	-7.64	0.331		0.331
$1h_{11/2}$	-7.54	0.224		0.224
$2d_{3/2}$	-7.31	0		0
neutron particle				^{133}Sn [20]
$2f_{7/2}$	-2.47	0		0
$3p_{3/2}$	-1.57	0.854		0.854
$1h_{9/2}$	-0.86	1.561		1.561
$2f_{5/2}$	-0.42	2.004		2.004
proton hole				^{131}In [19]
$2p_{1/2}$	-16.01	0.302		0.302
$1g_{9/2}$	-15.71	0		0
proton particle				^{133}Sb [20]
$1g_{7/2}$	-9.68	0		0
$2d_{5/2}$	-8.72	0.962		0.962
$2d_{3/2}$	-6.97	2.708		2.708
$1h_{11/2}$	-6.89	2.793		2.793
^{208}Pb				
neutron hole				^{207}Pb
$1h_{9/2}$	-11.40	4.036	0.98	3.400, 5.410, 5.620 [28]
$2f_{7/2}$	-9.81	2.439	0.95	2.340, 4.570 [28]
$1i_{13/2}$	-9.24	1.870	0.91	1.630, 5.990 [28]
$3p_{3/2}$	-8.26	0.89	0.88	0.890 [21]
$2f_{5/2}$	-7.94	0.57	0.60	0.570 [21]
$3p_{1/2}$	-7.37	0	0.90	0 [21]
neutron particle				^{209}Pb [22]
$2g_{9/2}$	-3.94	0	0.83	0
$1i_{11/2}$	-3.16	0.779	0.86	0.779
$1j_{15/2}$	-2.51	1.424	0.58	1.424
$3d_{5/2}$	-2.37	1.565	0.98	1.565
$4s_{1/2}$	-1.90	2.033	0.98	2.033
$2g_{7/2}$	-1.44	2.492	1.05	2.492
$3d_{3/2}$	-1.40	2.537	1.09	2.537
proton hole				^{207}Tl [29]
$1g_{7/2}$	-12.00	3.991	0.52	3.469, 3.995, 4.888
$2d_{5/2}$	-9.82	1.806	0.65	1.683, 4.696
$1h_{11/2}$	-9.36	1.348	0.88	1.348
$2d_{3/2}$	-8.36	0.351	0.90	0.351
$3s_{1/2}$	-8.01	0	0.85	0
proton particle				^{209}Bi [22]
$1h_{9/2}$	-3.80	0	1.00	0
$2f_{7/2}$	-2.90	0.897	1.38	0.897
$1i_{13/2}$	-2.10	1.697	0.93	1.612, 2.601
$2f_{5/2}$	-0.97	2.824	0.87	2.824
$3p_{3/2}$	-0.68	3.116	0.98	3.116
$3p_{1/2}$	-0.16	3.637	0.54	3.637

^a The data was extracted by systematic shell model studies of nuclei close to ^{100}Sn [30].

^b The data is based on the excitation energy of the lowest state of given spin and parity, no information on spectroscopic factors is available.

III. WOODS-SAXON CALCULATIONS

A. Woods-Saxon Hamiltonian

In this section, we develop the terms in the Woods-Saxon Hamiltonian from very general assumptions about the character of the nuclear mean field. For the most part, we arrive at the conventional Woods-Saxon Hamiltonian, but the purpose here is to emphasize the aspects of the mean field description and to emphasize the theoretical foundations behind the construction. We highlight the kinematic aspects of the problem and symmetry considerations. The concept of reduced mass and isospin-symmetry are of particular importance in the parameterization of the Woods-Saxon Hamiltonian introduced in this work.

The general strategy behind the construction of a center of mass Hamiltonian for the nuclear mean field starts with the assumption of a scalar interaction potential between nucleon and core as a sum of the nuclear and Coulomb parts. We assume the nucleon and a core forming a nucleus with mass number $A = N + Z$ containing N neutrons and Z protons. Thus the core has $A' = A - 1$ nucleons. In the following, we use the prime to denote quantum numbers and parameters of the core.

Woods and Saxon [3] suggested to model the nuclear mean field i.e. the nucleon-core interaction with a spherically symmetric potential that has a Fermi-function form

$$f(r, R, a) = \left[1 + \exp\left(\frac{r - R}{a}\right) \right]^{-1}, \quad (3)$$

where the size R and diffuseness of the surface a are fixed parameters of the same units of length as r .

The total nuclear potential is defined as

$$V(r) = -Vf(r, R, a), \quad (4)$$

where V represents total strength and the minus sign is introduced to represent the attractive nature of the interaction.

The electromagnetic force is a second part contributing to the proton-core interaction. This repulsive potential is fully determined with the assumption of a given nuclear charge distribution $\rho(r)$. The solution of the corresponding electrostatics problem gives

$$V_c(r) = 4\pi e \left(\frac{1}{r} \int_0^r r'^2 \rho(r') dr' + \int_r^\infty r' \rho(r') dr' \right). \quad (5)$$

In the spirit of the Woods-Saxon parameterization it is often assumed that the nuclear charge distribution is proportional in shape to the same function (3) $\rho(r) \sim f(r, R_c, a_c)$, where the coefficient of proportionality must be determined from the normalization of density to the total nuclear charge. The integration in Eq. (5) along with a normalization of density must be done numerically, which is often too time consuming. The influence

of surface terms on the strength of the Coulomb interaction is, however, weak. We have numerically tested, that the diffuseness of the charge distribution can be set to zero within the precision of the fit discussed below. Furthermore, for the same reason we have assumed $R_c = R$ which removes an extra unnecessary parameter that has little influence on the outcome. Except for special cases [7] these assumptions are typical in other Woods-Saxon parameterizations. Through this paper we adopt the following form of the Coulomb potential

$$V_c(r) = Z'e^2 \begin{cases} (3R^2 - r^2)/(2R^3), & r \leq R, \\ 1/r, & r > R, \end{cases} \quad (6)$$

which as a result of the above assumptions corresponds to a uniformly charged sphere of radius R , which can be treated analytically.

The understanding of the Woods-Saxon potential as a two-body problem naturally leads to the introduction of a reduced mass. However, in most previous treatments, notably [8], the bare nucleon masses were used in the kinetic energy term of the Hamiltonian. While the difference between a reduced or bare nucleon mass is not important for the bound state spectrum of heavy nuclides, its use would create serious problems for the description of light nuclides in our calculations, notably the nucleon orbitals around ^{16}O . Furthermore, we aim to apply this potential as a basis for continuum states, where the kinematic aspect becomes central. Thus, in the kinetic energy operator we use the following reduced mass

$$\mu = \left(\frac{1}{m_\nu} + \frac{1}{M'} \right)^{-1}, \quad (7)$$

where m_ν is a neutron/proton mass and M' is the mass of an $A - 1$ core, taken to be $(A - 1)amu$

In addition to the central and Coulomb potentials identified above, the relativistic corrections for a nucleon with a Fermi momentum of typically 200 MeV are important. In order to highlight the nature of these corrections, we give a non-relativistic reduction of the two-body Coulomb problem to the order of $(v/c)^2$. The correction to the nuclear potential is discussed below. The Dirac Hamiltonian reduces to

$$H = \frac{\mathbf{p}^2}{2\mu} - \frac{\mathbf{p}^4}{8\mu^3} + V_c(\mathbf{r}) + \frac{1}{4\mu^2} \sigma \cdot [\nabla V_c(\mathbf{r}) \times \mathbf{p}] + \frac{1}{8\mu^2} \nabla^2 V_c(\mathbf{r}). \quad (8)$$

Throughout this section, we use natural (Planck) units where $\hbar = c = 1$. In nuclei the contribution from the the second (kinetic energy) \mathbf{p}^4 term is small and therefore ignored. It turns out that, in comparison to nuclear forces, corrections due to Coulomb given by the last two terms are also small. For example the last so-called Darwinian term is constant, and only non-zero inside the uniformly charged sphere. For a typical nucleus its value $-3Z'e^2/(8R^3\mu^2)$ is only of the order of 20–30 keV which should be compared with ~ 50 MeV of a typical total

depth V in (4). It should also be stressed that terms of this nature can be subsumed in the phenomenologically determined parameters of the central potential. The spin-orbit contributions due to the Coulomb potential in eq. 8 are an order of magnitude smaller than the nuclear contributions and will be ignored.

Based on the previous discussion, only the nuclear spin-orbit contribution has to be included in descriptions of effective nuclear forces in addition to V_c . Eq. (8) is not valid as a relativistic reduction of the nuclear mean field problem due to the complicated structure of the nucleon-nucleon force. However, symmetry considerations suggest the same general proportionality of the spin orbit force to be the gradient of the mean field potential. Thus, the total effective Hamiltonian becomes

$$H = \frac{\mathbf{p}^2}{2\mu} + V(r) + V_c(r) + \frac{1}{2\mu^2 r} \left(\frac{\partial}{\partial r} \tilde{V}(r) \right) \mathbf{l} \cdot \mathbf{s}, \quad (9)$$

where – unlike for the Coulomb field – the potential $\tilde{V}(r)$ is not equal to the original potential $V(r)$ and may have a different form factor [31]. Therefore, the form factor of $\tilde{V}(r)$ is another assumption that goes into construction of the Woods-Saxon Hamiltonian

$$\tilde{V}(r) = \tilde{V} f(r, R_{SO}, a_{SO}). \quad (10)$$

Here, R_{SO} and a_{SO} stand for the radius and the diffuseness of the spin-orbit term.

In principle all symmetry preserving forces which involve the single particle operators \mathbf{p} , \mathbf{r} , \mathbf{s} , \mathbf{t} and the core spin and isospin operators \mathbf{T}' and \mathbf{I}' can appear in the particle-core parameterizations. These generally small terms are extensively discussed and studied within the optical model approach to reaction physics [32, 33]. The consideration of an odd-particle mean field that carries quantum numbers of an unpaired nucleon is beyond the goals of the parameterization discussed here. Therefore, we assume that the core generally carries no spin degree of freedom $I' = 0$. The only time such terms can be of relevance is when single-particle energies are to be extracted from hole states Eq. (1) in this case the particle spin may couple to identical single-hole quantum numbers of the core. These terms are generally small and have a $1/A$ dependence [5], just as in Eq. (13). The only “second-order” term of concern is a possible isospin-dependence of the spin-orbit strength i.e. $(\mathbf{T} \cdot \mathbf{t})(\mathbf{l} \cdot \mathbf{s})$. This dependence has been the subject of several studies [34, 35] as it represents one of the most interesting, fundamental and at the same time controversial questions related to the nuclear mean field. The example of a non-relativistic reduction of the Coulomb potential and the more rigorous studies using the Relativistic Mean Field approach suggest the same sign of isovector term in spin orbit potential as in the central. However, a substantial amount of experimental data [34, 35, 36] as well as theoretical understanding of an issue based on the Walecka model suggest the opposite. Namely, for the neutron rich nuclei the spin orbit splitting for the neutrons is larger than for

the protons. Those studies suggest the value $\kappa_{SO} \sim -0.3$ which can be compared to the typical strength of the isotopic term in the central potential $\kappa \sim 0.6$ to 0.9 ; see discussion below for details and definitions. The more in-depth arguments and understanding of the spin orbit splitting comes from studies of shell evolution due to the tensor forces [53]. The effects of the ρ meson exchanges in the nucleon-nucleon interaction are particularly important for these mean field properties.

We used our data set and fit procedure to assess the variation of spin-orbit strength with isospin. Unfortunately, as was already pointed out in Ref. [34, 36] the data based on single-particle energies is only weakly sensitive to this parameter. Within the precision of our study we were unable to distinguish any significant isospin dependence of the spin orbit term. Thus, with no better alternative we define the spin orbit strength in our parameterization with no explicit dependence on isospin.

B. Woods-Saxon parameterization

The Hamiltonian of the model is defined in Eq. (9), where the central potential is determined in Eq. (4) and the spin-orbit term is given by Eq. (10). Both central and spin-orbit parts have a Woods-Saxon form factor (3). The Coulomb part is given by Eq. (6). For each individual nucleus the Hamiltonian is determined by the following list of parameters R , a , V , R_{SO} , a_{SO} , \tilde{V} and the reduced mass μ ; these seven parameters *define* the Woods-Saxon potential.

The parameters of the potential change as one goes over the nuclear chart. The dependence of the above 7 parameters on the number of protons and neutrons in the core-nucleon problem defines the *structure of parameterization*. In the following, we will describe our choice of structure parameterization, which we call the “Seminole” parameterization.

In the conventional parameterization of the Woods-Saxon potential, as well as in our work, the size of nuclear potential is calculated as

$$R = R_C = R_0 A^{1/3}, \quad R_{SO} = R_{0,SO} A^{1/3}, \quad (11)$$

in terms of the parameters R_0 and $R_{0,SO}$, which are constant over the nuclear chart.

The surface diffuseness for both the central and spin-orbit potential is assumed to be constant and size independent

$$a = a_{SO} = \text{const.} \quad (12)$$

While the isospin dependence of the Coulomb force is obvious, the behavior of the effective nuclear potential on the isospin of the nucleon \mathbf{t} and the core \mathbf{T}' has to be introduced phenomenologically. We adopted the suggestion by Lane [37] to introduce an isospin dependence to the potential by the lowest order isospin invariant term

$$V = V_0 \left(1 - \frac{4\kappa}{A} \langle \mathbf{t} \cdot \mathbf{T}' \rangle \right). \quad (13)$$

We chose the “minus” sign so that the parameter κ will be consistent with conventions. For the ground-state of a nucleus, the isospin quantum number is $T = |T_z| = |N - Z|/2$, which together with the relation $\mathbf{t} + \mathbf{T}' = \mathbf{T}$ leads to

$$-4\langle \mathbf{t} \cdot \mathbf{T}' \rangle = \begin{cases} 3 & N = Z \\ \pm(N - Z + 1) + 2 & N > Z \\ \pm(N - Z - 1) + 2 & N < Z \end{cases}, \quad (14)$$

where here and below we use upper sign for the proton and the lower sign for the neutron. Traditionally, the isospin-dependence of the Woods-Saxon potential had been parameterized by the expression.

$$V = V_0 \left(1 \pm \kappa \frac{(N - Z)}{A} \right) \quad (15)$$

For heavy nuclei with large neutron excess, the difference between the two definitions is small. However, the definition of Eq. 14 leads to significantly different predictions in lighter nuclides around $N=Z$. We discuss the validity of this assumption for the description of our data in section IV.

The structure of the “Seminole” parameterization is given by Eqs. (13) and (14) which define the dependence of the potential depth on Z and N in an isospin conserving way.

The spin-orbit interaction strength is determined by

$$\tilde{V} = \lambda V_0, \quad (16)$$

using a proportionality constant λ which is a constant, making \tilde{V} a constant. This aspect of our parameterization is different from the traditional approach, where the spin orbit potential depth is modified with the same isospin dependent factor as the central potential. Finally, the reduced mass is given as in Eq. (7), where the mass of the core is parameterized as $(A - 1)u$. The 6 constants $V_0, R_0, R_{0,SO}, a = a_{SO}, \lambda$, and κ and are the actual parameters of the global “Seminole” Woods-Saxon fit.

We have also studied a possible variation of the potential radius with isospin. From our investigation of nuclear charge radii, which will be described in section IV C, we concluded that a modification of potential radii with respect to the standard structure of parameterization in Eq. (11) would lead to wrong predictions of experimental charge and neutron radii.

C. Existing parameterizations

A number of parameterizations and parameter sets are available in the literature. We list the most commonly used ones in Table III. All of these parameterizations use

Eq. (15) for the isospin dependence of the nuclear potential. In contrast to the “Seminole” parameterization, the same isospin dependence enters into spin-orbit term via

$$\tilde{V} = \lambda V, \quad (17)$$

which should be compared with Eq. (16).

The “Rost” parameters [38] were determined from the orbital energies of ^{208}Pb . The “Optimized” [39] parameter set took the central potential parameters from “Rost”, but changed the spin-orbit interaction in order to improve predictions for high-spin spectra in the lead region. A further refinement of these parameters was introduced as the “Universal” parameter set, which improved the description of high spin states in ^{146}Gd [8].

Common to these three parameterizations is the assumption of different parameters sets for the proton and neutron spectra, and specifically a larger neutron than proton potential radius. The implementation of these parameterizations through the computer code SWBETA [45] uses the the bare nucleon mass in the kinetic energy operator and a reduced mass $\mu = \frac{A-1}{A} u$ in the spin-orbit coupling potential.

IV. OPTIMIZATION OF WOODS-SAXON POTENTIAL PARAMETERS

A. Calculation of the Woods-Saxon spectrum and adjustment of parameters

Special attention had to be paid to the way in which the experimental particle and hole states are compared to the Woods-Saxon calculation. Single neutron states are naturally calculated as the potential for $(N_m + 1, Z_m)$, and single proton states as the $(N_m, Z_m + 1)$, where N_m and Z_m are the neutron and proton numbers of the respective magic core. The hole states around the same magic nucleus are nucleons moving in the field of a core, which has one nucleon less than the magic core, so that the orbitals based on hole states are calculated at (N_m, Z_m) .

As a primary computational tool, we used a Woods-Saxon code which is a part of the Continuum Shell Model code CoSMo discussed in [42] and that has been successfully used in studies of realistic nuclei [43]. Web implementation of this code for bound states along with the Seminole parameterization obtained as a result of this work can be found in [44]. The spectrum, radii, structure of wave-functions and reaction calculations were performed using this code which makes the current Woods-Saxon parameterization readily available for further incorporation into the Continuum Shell Model.

The independent use of the publicly available program SWBETA [45] to calculate the spectrum of the Woods-Saxon Hamiltonian provided a crucial verification. This program was modified slightly to incorporate the changes to the Woods-Saxon parameterization we introduced. Note that, while SWBETA calculates the spectrum of a

Parameterization		$V_0 [MeV]$	κ	R_0 [fm]	a [fm]	λ	R_{0SO} [fm]
'Rost'[38]	n	49.6	0.86	1.347	0.7	31.5	1.28
	p			1.275		17.8	0.932
'Optimized'[39]	n	49.6	0.86	1.347	0.7	36	1.30
	p			1.275		36	1.30
'Universal'[8]	n	49.6	0.86	1.347	0.7	35	1.31
	p			1.275		36	1.32
'Chepurnov'[40]		53.3	0.63	1.24	0.63	23.8 *	1.24
'Wahlborn'[41]		51	0.67	1.27	0.67	32	1.27

Table III: Commonly used Woods-Saxon parameter sets in the literature. * The ‘‘Chepurnov’’ parameterization introduced an additional isospin-dependence for the spin-orbit interaction in deviation from the commonly used proportionality to the central potential.

deformed Woods-Saxon potential, zero deformation was used for all calculations presented here.

We also developed a parameter fit program, which calls the Woods-Saxon calculation through a shell command with the hypothetical fit parameters and reads back the calculated orbital spectrum. The actual parameter optimization is realized through a Levenberg-Marquardt algorithm [46], which minimizes the χ^2 between the experimental and calculated orbital energies by systematically varying the potential parameters.

While the spectrum of all nuclides listed in section II was usually fit with the same set of parameters, the fit program also can allow for certain parameters to vary for each individual nuclide. This option was used to systematically investigate how to improve the dependence of certain parameters on the nuclide mass or the neutron-proton asymmetry.

Armed with a fitting procedure we first consider a structure of the ‘‘Universal’’ parameterization and fit its nine parameters to our data set of orbital energies around ^{16}O , ^{40}Ca , ^{48}Ca , ^{56}Ni , ^{100}Sn , ^{132}Sn and ^{208}Pb . The resulting parameters called ‘‘Fit A’’ are listed in table IV together with results from the ‘‘Universal’’ parameters. We observe that the large difference in central potential radius between neutron and proton radii disappears in the fit, although these parameters were free to adjust independently. The spin-orbit strength parameter λ is the only parameter in ‘‘Fit A’’ displaying substantially asymmetric values for neutrons and protons. Table IV also lists the RMS energy deviation obtained for the different nuclides. The ‘‘Fit A’’ parameters show a more consistent description of the lighter nuclei than the ‘‘Universal’’ parameters and a better description of the nuclides with $N=Z$. The features of ‘‘Fit A’’, namely a symmetric parameterization for protons and neutrons, serve as a guide to find an improved parameterization and parameter set addressed below. ‘‘Fit B’’, which is included in the table will be discussed in the following section.

B. Changes to the parameterization

In this paragraph we investigate the validity of the isospin-conserving parameterization introduced in

Eq. (14). In the procedure listed as ‘‘Fit B’’ in table IV, we introduced the reduced mass of Eq. (7), and the constant spin-orbit potential strength of equation (16). The central potential depth was optimized with a separate value for each neutron and proton, particle and hole data set in each nuclide, a total of 28 values. The other parameters R_0 , $R_{0,SO}$, a and a_{SO} were free to adjust one common value for all nuclides. The extracted V values are displayed in Fig.1, plotted as a function of the isospin multiplier $-\frac{4}{A}\langle \mathbf{t} \cdot \mathbf{T}' \rangle$. The values show a linear dependence on the isospin factor, in agreement with the parameterization (14). The only significant deviations from the linear dependence are found for both the particle ($\frac{4}{A}\langle \mathbf{t} \cdot \mathbf{T}' \rangle = 0, V_0 = 49.8 \text{ MeV}$) and hole orbitals ($\frac{4}{A}\langle \mathbf{t} \cdot \mathbf{T}' \rangle = 0.1875, V = 57.3 \text{ MeV}$) of Oxygen. These data points are an indication that for lighter nuclei a reduced potential depth would improve the fit quality. However, we did not introduce a mass dependence to the potential depth parameter for the sake of simplicity and a more stable extrapolation.

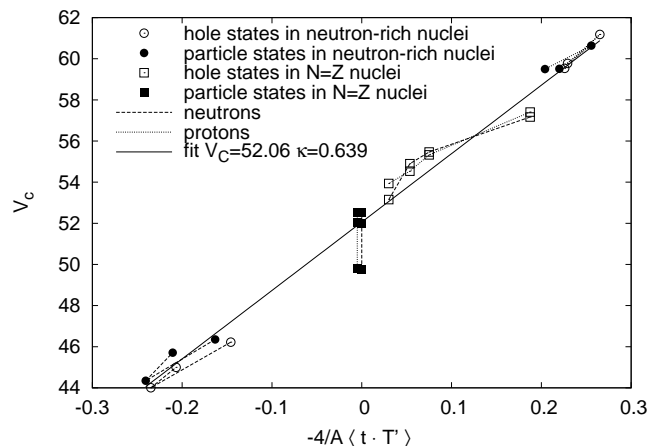


Figure 1: Central potential strength extracted from ‘‘Fit B’’ as a function of the isospin factor $-\frac{4}{A}\langle \mathbf{t} \cdot \mathbf{T}' \rangle$ (see Eq. 14). The straight line represents the central potential parameterization assumed in this work.

The question, whether the spin-orbit potential depends on isospin was investigated by allowing a modification in analogy to the isospin-dependence of the central po-

		V_0 [MeV]	κ	R_0 [fm]	a [fm]	λ	R_{OSO} [fm]	RMS energy deviation [MeV]						
								^{16}O	^{40}Ca	^{48}Ca	^{56}Ni	^{100}Sn	^{132}Sn	^{208}Pb
Univ.	n	49.6	0.86	1.347	0.7	35	1.31	2.65	1.68	1.07	1.18	1.20	0.40	0.37
	p			1.275		36	1.32	2.31	2.18	1.63	1.40	2.29	0.61	0.43
Fit A	n	52.78	0.636	1.282	0.62	24.0	1.18	1.91	0.84	1.06	0.55	0.72	0.53	0.60
	p			1.288		21.2	1.05	1.96	0.69	0.64	0.44	1.31	0.43	0.38
Fit B	var		0.000	1.260	0.68	25.5	1.21	0.33	0.52	1.34	0.45	0.74	0.53	0.40
	var								0.32	0.58	0.76	0.39	1.19	0.34

Table IV: Parameters and fit quality of the “Universal” parameterization compared to parameter fit “Fit A” adjusting the same parameters to the orbital energy data presented in section II. In “Fit B” parameters labeled “var” were allowed individual values for each nuclide for protons, neutrons, for particle and hole state (see text). The individual parameter values are displayed in Fig. 1. The values of the other parameters were allowed to adjust one common value during the fit, with the exception of κ , which was held constant at 0.

tential. Note that in the previous parameterizations [8], the spin orbit potential strength was assumed to be directly proportional to the central potential, thus having an explicit isospin-dependence. As was stated earlier the isospin-dependence of a spin-orbit term, although an interesting question, can not be fully addressed with our approach. All our attempts to adjust this parameter led to a slight deterioration of the fit with most effects due to the $(\mathbf{T} \cdot \mathbf{t})(\mathbf{I} \cdot \mathbf{s})$ term being subsumed in the adjustment of the other parameters. Therefore, we defined our parameterization as not containing this term. We believe that this feature given its marginal and elusive effect on the single particle bound and resonant spectra is not essential for our purpose. In fact the isospin dependence in the spin orbit is a weak manifestation of the physics that goes beyond the mean field and thus it should be treated using a more advanced approach such as shell model based on the Woods-Saxon basis from our parameterization. Furthermore, the reduced number of free parameters allows us to achieve a more stable parameterization.

C. Charge Radii

While the description of the orbital energy spectra is an important component of any model of single particle motion, the Woods Saxon potential also strives to reproduce the geometry of the nucleus and properties that are sensitive to the geometry of its wave functions. Especially since the radial and potential depth values parameters show strong correlations in their influence on the particle energy spectrum, it is important to study the geometric properties of the wave-functions in an independent fashion.

We took data on experimental rms charge radii from the compilation by I. Angeli [47], for the proton-magic nuclides ^{16}O - ^{18}O , ^{40}Ca - ^{50}Ca , ^{108}Sn - ^{115}Sn and ^{190}Pb - ^{213}Pb . Using our new parameterization, we calculated the RMS radii of the same nuclides by averaging in square all proton orbital radii with their proper occupation numbers up to the Fermi level. To the orbital RMS radius, the RMS radius of the proton was added in square by

$$R_{charge} = \sqrt{R_{orbit}^2 + R_{proton}^2}.$$

The experimental charge radii, the results obtained for our parameters and the results for the “Universal” parameters are displayed in Fig. 2. Note that for each isotopic chain displayed here, the protons occupy the same orbitals, so that the observed variations are due to changes in the orbital geometry only.

We varied the potential radius parameter for values between 1.25 and 1.29 fm, while adjusting the other potential parameters for each step to reproduce the orbital energy data. The value of $R_0 = 1.26$ fm best reproduces the charge radii for the ^{190}Pb - ^{208}Pb isotopes. The increase of experimental charge radii observed beyond ^{208}Pb has been discussed in the context of various models, most recently in a systematic discussion of quadrupole correlation effects in a self-consistent calculation with the SLy4 interaction [48]. Our much simpler model can not reproduce this increase, either. The Tin and Calcium isotopes exhibit slightly larger rms radii than calculated. It is likely that this deviation is due to an onset of deformation in mid-shell, consistent with the calculations of [48].

It should be noted, that the variation of rms radii within the isotopic chains is determined only in part by the global scaling of the potential radius with $A^{1/3}$. Clearly evident in the data is a systematic dependence on the binding energy of the fermi orbital, where proton-rich nuclides have relatively larger charge radii than expected from the global scaling of the potential radius. Our calculations illustrate, that the same orbitals occupy a larger fraction of the potential radius as they become less bound.

Direct data on the neutron radii is much harder to obtain; However, some information on the relative radii of neutrons and protons can be deduced from isovector spin-dipole resonances, studied e.g. with the ($^3\text{He}, t$) reaction at intermediate energies. In Ref. [49], the authors extracted values for the difference between neutron and proton rms radii for even-mass Tin nuclides, which we display in Fig. 3, along with the values calculated for our Woods-Saxon parameterization and the “Universal” parameterization. The data presented in the figure supports the assumption of symmetric proton and neutron potential radii rather than the relatively larger neutron

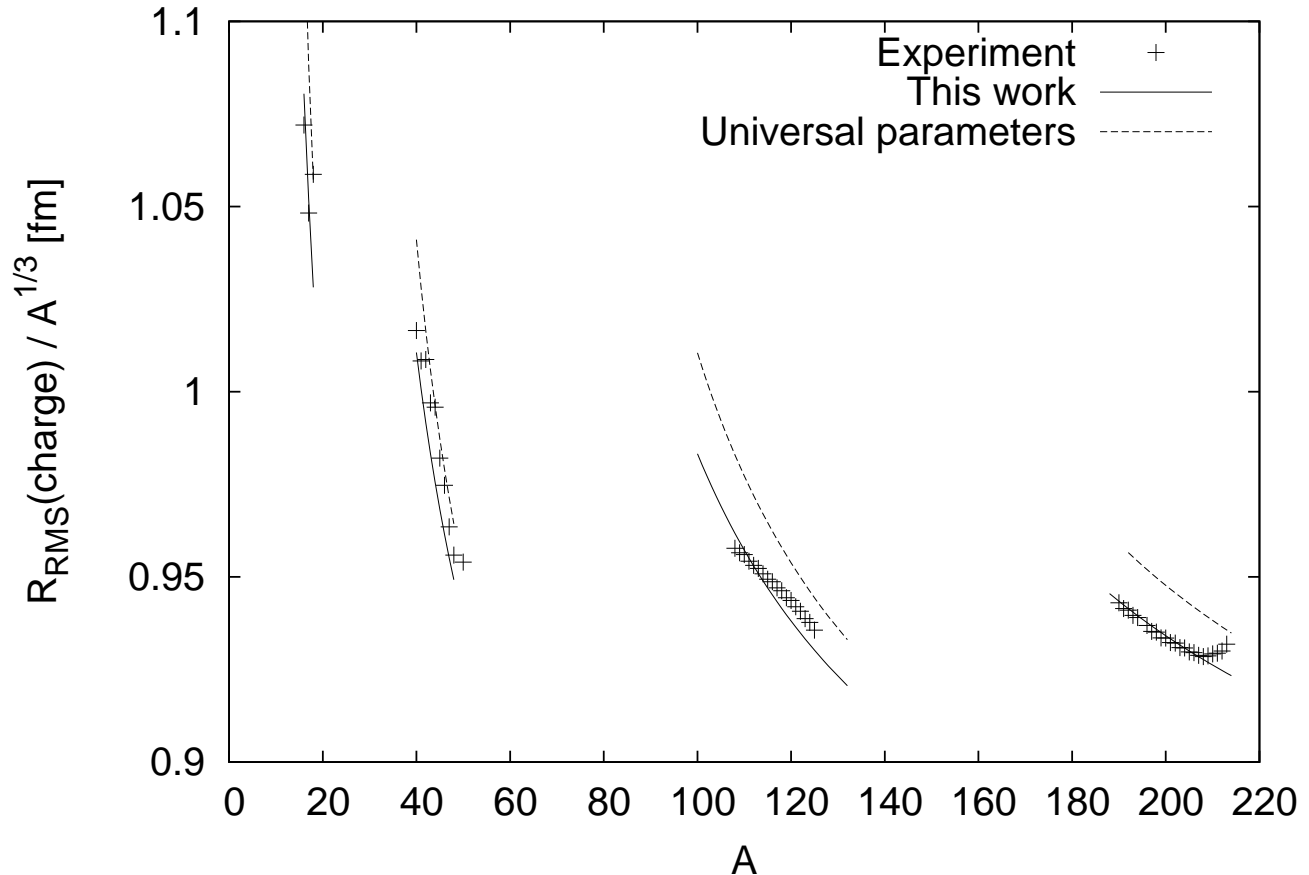


Figure 2: Experimental rms charge radii divided by the scaling factor $A^{1/3}$ as a function of mass number (symbols), for a set of Oxygen, Calcium, Tin and Lead isotopes. The data is compared to the results calculated with our parameters (solid line) and the “Universal” parameters (dashed line). The experimental uncertainties are typically smaller than 0.005 fm.

potential of the “Universal” parameterization.

V. THE NEW WOODS-SAXON POTENTIAL PARAMETERIZATION

A. The Parameters

We arrive at the structure parameterization given by Eqs. (7), (11)-(16). The corresponding parameters were adjusted to the orbital energy data. Their values are displayed in table V

V_0 [MeV]	κ	R_0 [fm]	$a = a_{SO}$ [fm]	λ	$R_{0,SO}$ [fm]
52.06	0.639	1.260	0.662	24.1	1.16

Table V: Woods-Saxon potential parameter set obtained in this work.

Summarizing, the important properties of the parameterization and the parameter set are:

- Reduced mass in the form given by Eq. (7) assures correct two-body kinematics of nucleon and

core. The average mass per nucleon in a nucleus is assumed to be equal to an atomic mass unit $u = 931.49 \text{ MeV}/c^2$. The introduction of the reduced mass led to a substantial improvement in the quality of description for the Oxygen and Calcium spectra.

- Identical potential parameters for neutrons and protons, which in conjunction with Eq. (13) assures isospin conservation.
- The spin-orbit term is constant and does not depend on isospin.
- There are only six parameters that were fitted. These parameters are given in table V.

B. Discussion of Fit Results

The experimental and calculated orbital energy spectra are displayed in figures 4-10. We will first address the spectra of the symmetric $N=Z$ nuclides ^{16}O , ^{40}Ca , ^{56}Ni and ^{100}Sn . For these nuclides, the spectrum calculated

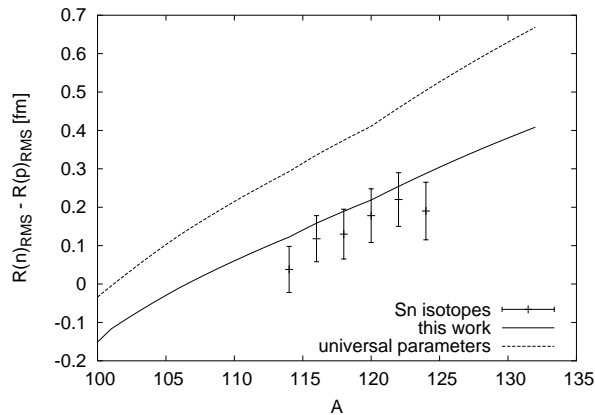


Figure 3: Values for the difference between the neutron and the proton rms radii in Sn isotopes, extracted from experimental data in spin-dipole resonances [49] (symbols). The data is compared to the results calculated with our fit parameters (solid line) and the “Universal” parameters (dashed line).

with the “Universal” parameterization shows consistently too small neutron and proton energy gaps around the magic numbers 8,20,28 and 50. The new parameterization greatly improves the accuracy of the orbital spectrum description.

As mentioned in section III, the “Universal” parameterization was primarily developed from the spectrum of ^{208}Pb . It is therefore not surprising that it is less applicable to symmetric $N=Z$ nuclides, especially since it is based on substantially different neutron and proton potential parameters. The “Universal” parameters fare better with the neutron-rich nuclides ^{48}Ca , ^{132}Sn and ^{208}Pb , which all have similar neutron-excess values of $(N - Z)/A = 0.167, 0.242$ and 0.212 , respectively. In general, the description of these nuclides by the new parameters is of similar quality as the “Universal” parameterization, with one exception – although the RMS deviation of the neutron particle spectrum of ^{208}Pb with the new parameters (0.5 MeV) is similar to the one obtained from the “Universal” parameters (0.37 MeV), the new parameter spectrum calculates all neutron “particle” orbitals systematically less bound than the experimental values. The magnitude of these deviations is not beyond the typical discrepancies of individual orbital fits in other nuclides, so that we do not think it represents a systematic problem within our parameterization. It should also be noted, that we could not find experimental information on the fragmentation of the single-particle strength for the nuclide in question, ^{209}Pb , in the literature. If we assume that the orbital fragmentation of high-lying states in ^{209}Pb is similar to that of the neutron hole orbitals in ^{207}Pb , the systematic “under-binding” of our description would vanish.

VI. PREDICTIONS OF SHELL STRUCTURE IN EXOTIC NUCLIDES

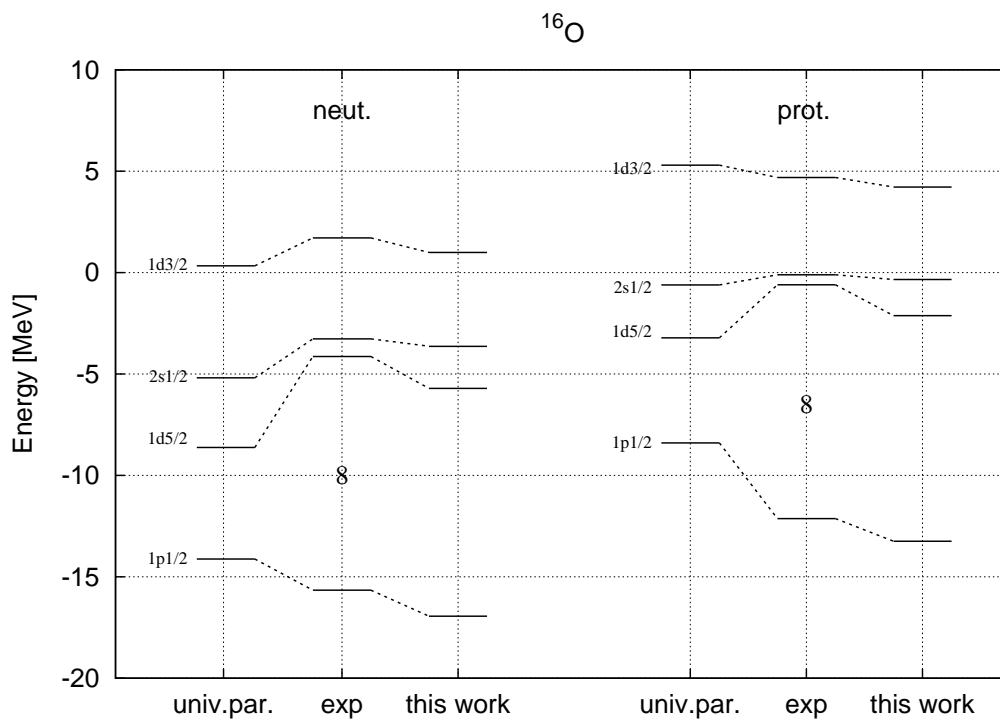
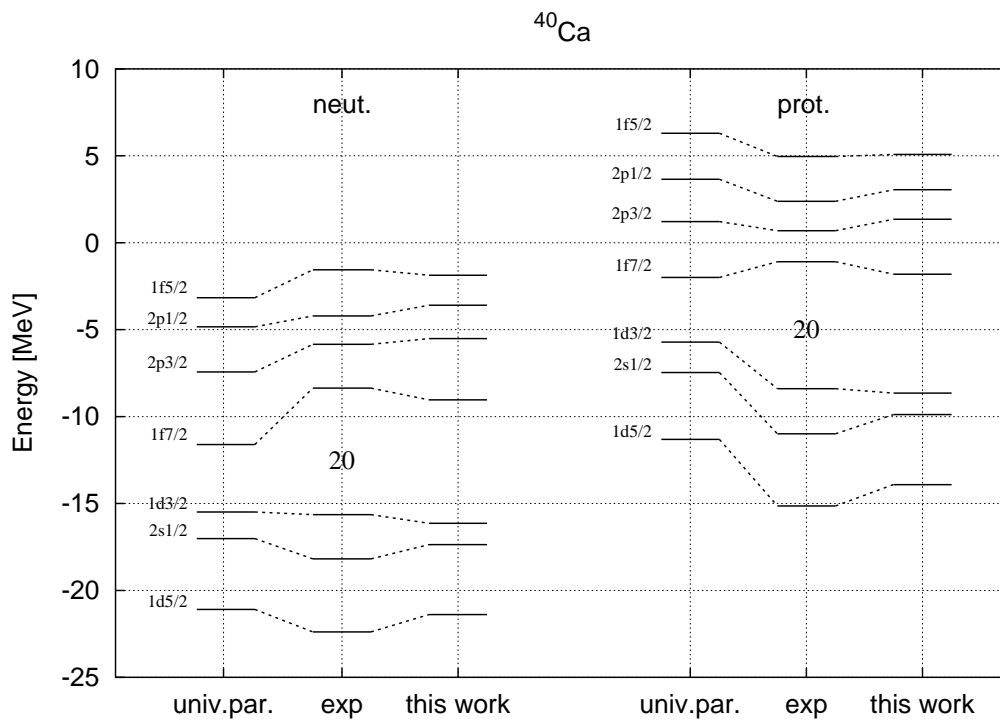
The discussion of all consequences of our new parameterization for the Woods-Saxon potential is clearly beyond the scope of this paper. The reader may further explore the features of this parameterization using our web-based program [44]. Here, we want to briefly discuss the general properties of the shell structure for exotic nuclides and the limits of nuclear binding it implies. We use the “Seminole” parameterization to calculate shell gap energies by filling the orbitals to the Fermi level and calculating the energy gap to the next unoccupied orbital for all nuclides between $Z=8$ and $Z=150$. Table VI lists the nuclides, for which a shell gap of at least 1.5 MeV is present for both neutrons and protons and for which both protons and neutrons were calculated to be bound. Note, that in this table, the gap is calculated from the orbital energy differences within one potential calculation, while the data represented in each of the figures 4–10 corresponds to two calculations, one for the core and one for the odd-nucleon neighbor, which leads to slightly different shell-gap values. Table VI also lists the neutron and proton separation energy, calculated as the binding energy of the Fermi level. Experimental values are taken from the compilation of [50].

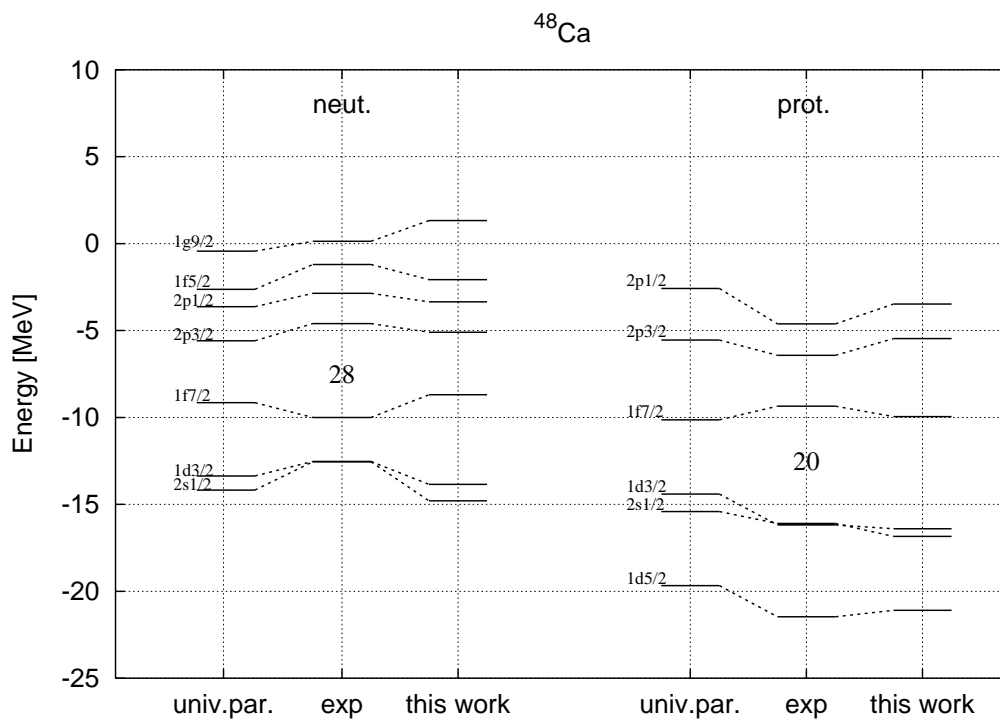
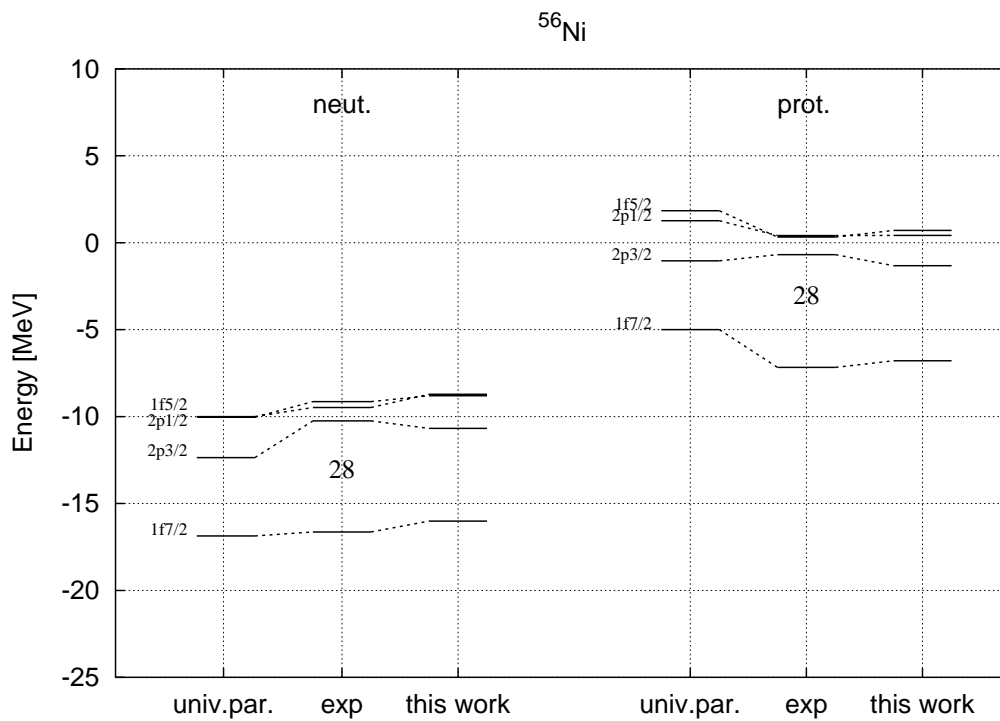
The data for nuclides between $Z=8$ and $Z=51$ is also represented as a nuclear chart in Figure 11. For nuclides with doubly closed sub-shells, the minimum of the respective proton and neutron shell gaps is represented by shades of red. The nucleon numbers of sub-shell closures are indicated by thin lines. All other nuclides are represented by shades of cyan color, which indicates the minimum of separation energy in protons and neutrons. We also draw the calculated limits of nuclear binding.

We find it necessary to stress again that Woods-Saxon parameterization is a very crude approximation to the nuclear mean field; The true potential can be quite different (the possibility of deformation is particularly noteworthy) and could include more complicated spin and tensor structures. Furthermore the parameters of potential can change as a function of N and Z in a non-uniform manner [51]. Although our potential is intended for use as a part of a more involved many-body approach it is still instructive to explore the shell evolution due to mere geometric modification that appear in our parameterization.

A. $N=16$ and $N=20$ Shell Closures

The modification of shell structure in exotic nuclides is currently a topic on which great experimental and theoretical efforts are expended. Otsuka and co-workers have attributed a significant renormalization of shell model single-particle energies to scalar [52] and tensor [53] components of the spin-spin proton-neutron residual interaction. These interactions act mainly on the spin-orbit

Figure 4: Orbital energy spectrum for ^{16}O .Figure 5: Orbital energy spectrum for ^{40}Ca .

Figure 6: Orbital energy spectrum for ^{48}Ca .Figure 7: Orbital energy spectrum for ^{56}Ni .

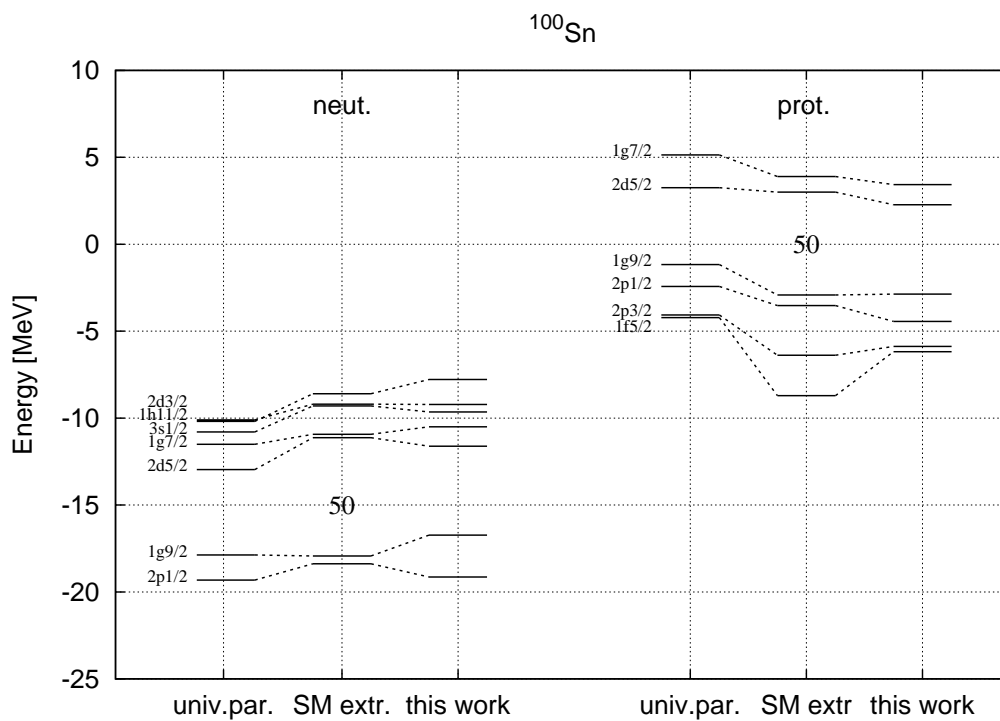


Figure 8: Orbital energy spectrum for ^{100}Sn . The data in the center column is extracted from systematic Shell-model calculations of nuclides approaching ^{100}Sn [30].

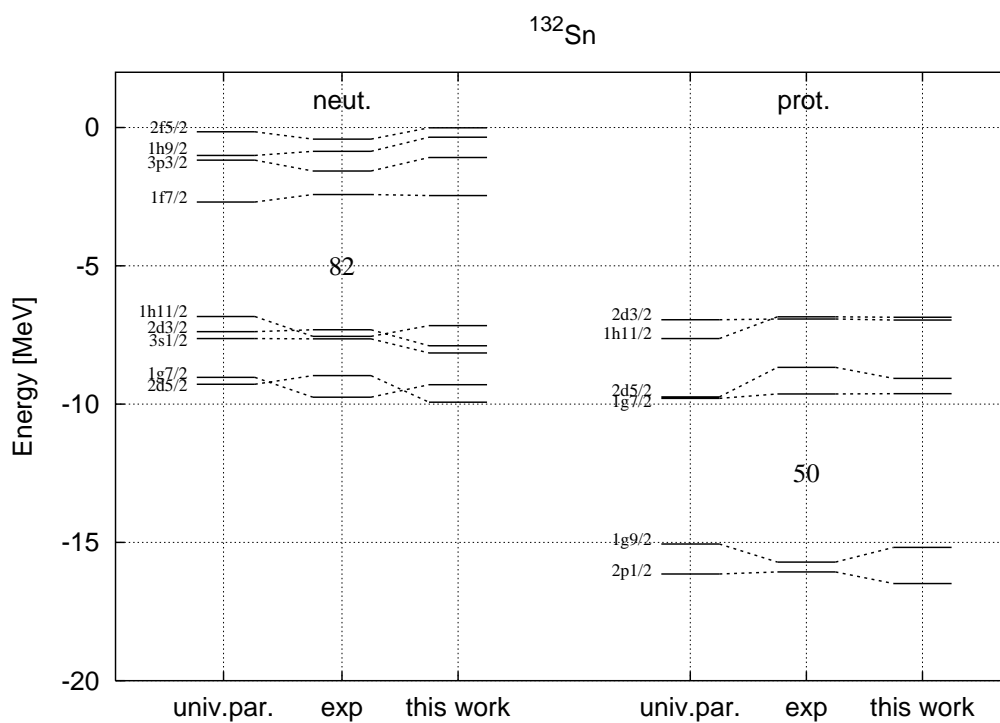


Figure 9: Orbital energy spectrum for ^{132}Sn .

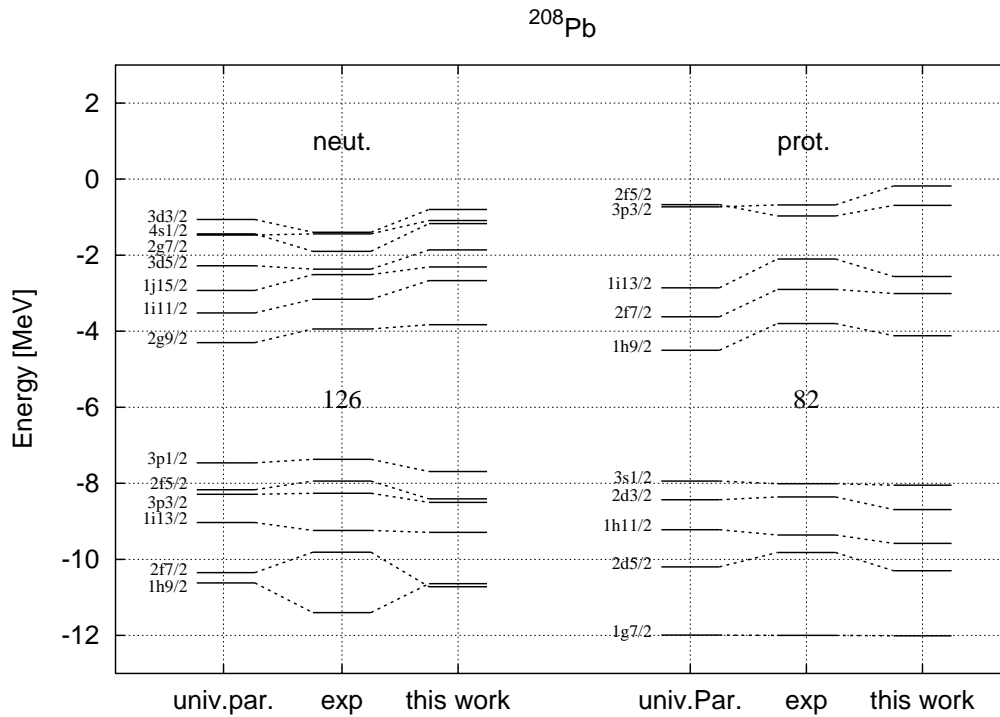
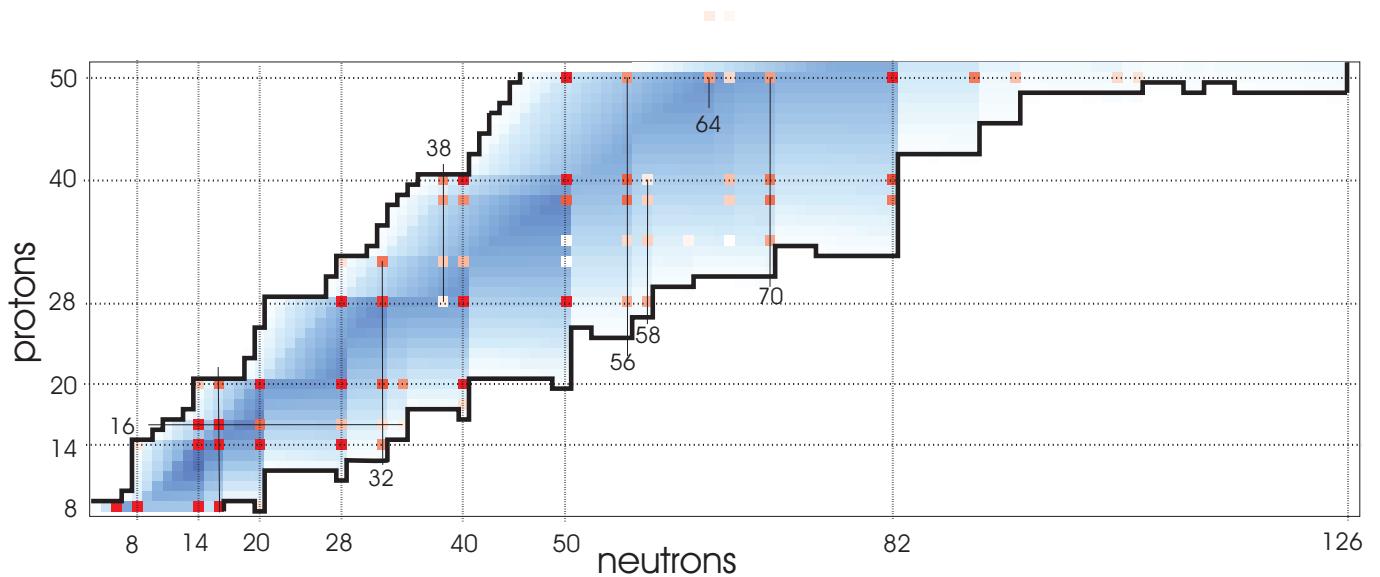
Figure 10: Orbital energy spectrum for ^{208}Pb .

Figure 11: Nuclear chart representing the calculated shell gaps, nucleon separation energies and drip-lines of nuclides between nuclides of $Z=8$ and $Z=51$. For doubly sub-magic nuclei, which are located at the crossing points of the dotted lines, the minimum of the proton and neutron shell gaps is represented by the shade of red, where larger gaps correspond to a deeper color. All other bound nuclides are represented by a shade of cyan color, which represents the minimum of the proton and neutron separation energies. The calculated proton and neutron drip-lines are also drawn.

	N	Z	WS Gap _N [MeV]	WS Gap _P [MeV]	WS S _N [MeV]	WS S _P [MeV]	exp S _N [MeV]	exp S _P [MeV]
¹⁴ O	6	8	5.64	7.01*	23.80	5.57	23.18	4.63
¹⁶ O	8	8	8.97	8.56	16.93	13.24	15.66	12.13
²² O	14	8	2.23	9.58	5.58	24.78	6.85	23.26
²⁴ O	16	8	3.51*	9.68	3.29	27.78	3.6	26.6**
²⁸ O	20	8	3.82*	9.75	0.23	32.88		
²⁸ Si	14	14	3.81	3.71	16.22	10.67	17.18	11.58
³⁰ Si	16	14	2.39	3.95	10.58	13.27	10.61	13.51
³⁴ Si	20	14	5.12	4.24	7.94	17.94	7.53	18.72
⁴² Si	28	14	2.23	4.44	3.20	25.50	3.20**	24.56**
³⁰ S	14	16	3.97	2.46	18.78	4.51	18.98	4.40
³² S	16	16	2.04	2.02	14.23	8.07	15.04	8.86
⁴⁰ Ca	20	20	5.95	5.43	16.15	8.66	15.64	8.33
⁴⁸ Ca	28	20	3.53	5.95	8.71	16.39	9.94	15.86
⁵² Ca	32	20	1.67	6.10	5.02	19.67	4.72	17.80**
⁶⁰ Ca	40	20	2.96*	5.95	2.53	24.96		
⁷⁰ Ca	50	20	2.22*	5.63	0.25	30.25		
⁵⁶ Ni	28	28	4.44	4.35	16.01	6.79	16.64	7.17
⁶⁸ Ni	40	28	3.29	4.97	8.16	14.86	7.79	15.69
⁷⁸ Ni	50	28	3.55	5.13	5.04	20.30	5.62**	
⁸⁸ Sr	50	38	4.53	1.57	10.50	10.62	11.12	10.61
⁸⁰ Zr	40	40	2.92	2.29	15.49	3.20	16.23	4.44
⁹⁰ Zr	50	40	4.66	2.06	11.53	8.19	11.97	8.35
⁹⁶ Zr	56	40	1.57	1.96	6.68	10.91	7.86	11.52
¹²² Zr	82	40	3.98*	1.69	3.38	20.60		
¹⁰⁰ Sn	50	50	5.15	5.61*	16.74	2.87	17.65**	2.80*
¹³² Sn	82	50	4.75	5.23	7.19	15.16	7.31	15.71
¹⁴⁶ Gd	82	64	5.27	1.69	12.04	4.72	11.2	5.38
¹⁸² Pb	100	82	1.53	4.43*	11.04	2.01	11.75	1.31
²⁰⁸ Pb	126	82	3.88	3.64	7.69	8.00	7.37	8.01
²¹⁸ U	126	92	3.82	1.16	9.81	1.78	8.85	2.43
²⁵⁶ U	164	92	1.37	1.68	5.06	9.64		
²⁷⁶ U	184	92	2.39	1.81	2.68	13.11		
²⁷⁸ 114	164	114	1.98	1.97	9.28	2.19		
²⁹⁸ 114	184	114	2.84	1.87	6.10	5.41		
³⁴² 114	228	114	2.09	1.70	3.14	11.50		

Table VI: Table of nuclides with a Fermi level shell gap calculated larger than 1.5 MeV in both protons and neutrons by the ‘‘Seminole’’ parameterization. Cases where the upper orbital for the shell gap was calculated to be unbound are marked with an asterisk. The following columns list the calculated neutron and proton separation energies and the experimental separation energies from [50]. Values marked with two asterisks are based on extrapolation, not experiment. More calculations may be performed using our program at [44].

partners of protons and neutrons. For instance, as the proton $d_{5/2}$ occupation goes from 6 protons at $^{30}_{14}\text{Si}_{16}$ to zero for the $^{24}_8\text{O}_{16}$, the effective orbital energy for the neutron $d_{3/2}$ orbital is calculated to increase. This effect creates a N=16 shell gap at the neutron drip line and also leads to the breaking of the N=20 magic number in the ‘‘island of inversion’’ around ^{32}Mg .

Our model naturally includes halo phenomena of weakly bound states, as observed in the charge radii displayed in Fig. 2. In consequence, the increased radial extension leads to modifications in the spin-orbit split-

ting. The corresponding (sub)-shell gaps for the above mentioned example are included in table VI – the calculated N=16 shell gap increases from 2.43 MeV in ^{30}Si to 4.51 MeV in ^{24}O , while the N=20 gap decreases from 5.09 MeV to 3.82 MeV between ^{34}Si and ^{28}O .

We conclude that some modifications of shell structure in exotic nuclides can be explained by a model as simple as the presented Woods-Saxon potential, as it includes quantum-mechanical dynamics of weakly bound particles. In our results however, the size of the N=16 shell gap does not reach the ≈ 6 MeV calculated in [52].

B. N=28 and Z=14 Shell Closures

The question, whether also the N=28 shell closure is broken in neutron-rich nuclides is another topic of intense investigations and discussion. Here, the mechanics of a possible breaking of the N=28 gap would be different from the N=20 case discussed above – since the N=28 closure is based on the $f_{7/2}$ orbital and the proton $f_{5/2}$ remains empty for the neutron-rich as well as the stable N=28 nuclides.

The Woods-Saxon potential calculation shows a clear decrease of the N=28 gap as we compare the values for the increasingly exotic ^{56}Ni , ^{48}Ca and ^{42}Si , at 4.44 MeV, 3.53 MeV and 2.22 MeV, respectively (see Tab.VI). Based on expectations of a decreasing N=28 shell gap, several theoretical investigations [54]–[57] had predicted a strongly deformed ground state in $^{42}_{14}\text{Si}_{28}$. However, in an experiment of one- and two-proton knockout reactions with a ^{44}S beam, it was shown that there is a substantial Z=14 shell closure [58, 59] and nearly degenerate $s_{1/2}$ and $d_{3/2}$ orbitals. The shell gap data listed in table VI and represented in Fig. 11 supports these findings; The calculated Z=14 sub-shell gap increases from 3.68 MeV in the stable ^{28}Si to 4.42 MeV in ^{42}Si . Our calculation also shows the near degeneracy of the $s_{1/2}$ and $d_{3/2}$ orbitals, which here are calculated only 0.63 MeV apart. Note that this orbital spacing is also present in the ^{48}Ca data displayed in figure 6. This spacing generates a large Z = 14 gap and a very small Z = 16 gap, which is consistent with a magic character of ^{42}Si with a stabilized N=28 closure and a moderate deformation ^{44}S , as observed in [60, 61].

C. Limits of Nuclear Binding

The limits of neutron binding and location of the neutron drip-line is a very important property of atomic nuclei, which is largely unknown at this time. The location of the neutron dripline has implications for the nucleosynthesis of heavy elements in the universe as well as for the physics of neutron stars. Radioactive beam facilities of the next generation are designed to establish the limits of neutron binding as one of their central goals.

We therefore want to discuss some of the straightforward implications of our Woods-Saxon parameterization for the limits of nuclear binding. It is clear that a model like the Woods Saxon-potential does not include residual interactions and therefore a lot of interesting physics is out of reach for this approach. Nevertheless it can serve as the first order approximation in the determination of the drip lines and the basis for more detailed theoretical investigations.

The calculated proton and neutron drip-lines are displayed in Fig.11 and clearly show the effect of shell and sub-shell closures. Interestingly, the neutron drip-line shows a number of instances, e.g. the Ca isotopes, where the presence of magic numbers leads to regions, where an element has bound nuclides after unbound ones. This “meandering” of the neutron drip line does not occur for the proton drip line.

Oxygen is the heaviest element, for which the location of the neutron drip line is known at the present time. Experiments with high sensitivity have established, that ^{26}O is unbound [62, 63]. Our calculation, represented in Fig. 11 also shows ^{26}O to be unbound, but brings back ^{28}O as a nuclide bound by 0.21 MeV due to the $N=20$ shell closure.

The Tin isotopes are calculated to be neutron-bound up to ^{176}Sn . We display the calculated and experimental neutron separation energies for the odd-neutron Sn isotopes in Fig.12. A surprising property of the calculated energies is the almost constant, very low neutron separation energy of the Fermi orbital from $N=93$ up to the $N=126$ shell closure. This property is based on a large number of orbitals being situated very close to the Fermi energy— ^{176}Sn binds 34 neutrons within an energy interval of 0.84 MeV. For comparison, the same number of neutrons in the same orbitals is spread out over an energy interval of 3 MeV in the spectrum of ^{208}Pb . The large number of orbitals in a small energy interval will make it very difficult to predict the neutron drip-line in the Sn-isotopes by theoretical means and shows the need for experiments with very exotic nuclides. The situation of orbitals is analogous to the one in neutron rich Zirconium isotopes with $A>122$, which was shown to lead to giant halos in relativistic Hartree-Bogoliubov calculations [64]. This property should make the neutron-rich Sn nuclides a very interesting system to study new modes of collectivity based on the interaction with the continuum.

VII. CONCLUSION

We have established a new parameterization for the Woods-Saxon potential. Its six parameters are fitted to

single-particle spectra around doubly magic nuclides and experimental charge radii. We achieved a high quality of description of the single-particle spectra observed around the doubly-magic nuclei between ^{16}O and ^{208}Pb . The nuclear properties such as radii, shell evolutions, magic

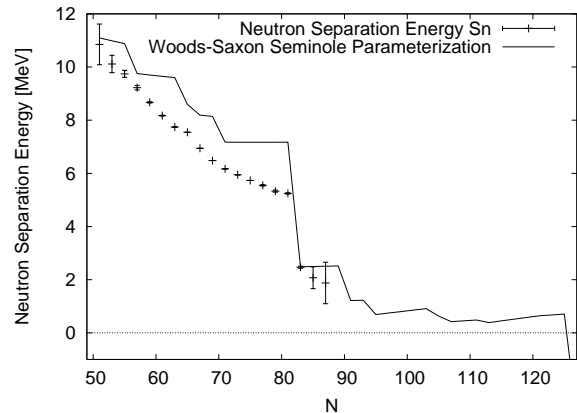


Figure 12: Neutron separation energies for odd-N Tin isotopes, calculated with the “Seminole” parameterization of the Woods-Saxon potential and experimental values from [50].

numbers and driplines are all shown to be well described considering limitations of the Woods-Saxon approach. The isospin conservation by the nuclear part of interaction and proper treatment of the two-body particle-core kinematics are important for the success of the model. The parameter set is intended to enable the use of the Woods-Saxon potential as a basis for shell model calculations and a pathway to connect the physics of bound and unbound nuclear states.

VIII. ACKNOWLEDGEMENTS

We would like to acknowledge the numerous discussions and contributions by Prof. R.A. Wyss and Dr. A. Oros in a previous effort to determine an optimized parameter set for the Woods-Saxon potential. This work was supported partially by the NSF under contract No.0456463 and by the DOE under contracts DE-FG02-02ER41220 and DE-FG02-92ER40750.

[1] M. Goeppert-Mayer, Phys. Rev. **75**, 1969 (1949).

[2] B.A. Brown and B. Wildenthal *Ann. Rev. Nucl. Part.*

- Sci.* **38**, 29 (1988); B.A. Brown *Prog. Part. Nucl. Phys.* **47** 517 (2001).
- [3] R.D. Woods and D.S. Saxon, *Phys. Rev.* **95**, 577 (1954).
- [4] J.N. Ginocchio, *Ann. Phys.* **152**, 203 (1984); **195**, 467 (1985).
- [5] H. Feshbach, *Annu. Rev. Nucl. Sci.* **8**, 49 (1958).
- [6] N. Michel *et.al.* *Phys. Rev. Lett.* **89** 042502 (2002); *Phys. Rev. C* **67** 054311 (2003); *Phys. Rev. C* **70** 064313 (2004).
- [7] H. Esbensen and C. N. Davids, *Phys. Rev. C* **63**, 014315 (2001).
- [8] J. Dudek, Z. Szymanski, T. Werner, A. Faessler and C. Lima: *Phys. Rev.* **C26** 1712 (1982)
- [9] Z. Lojewski, B. Nerlo-Pomorska, K. Pomorski, J. Dudek, *Phys. Rev. C* **51**, 601 (1995)
- [10] B.Cederwall *et al.* *Phys.Rev.Lett.* **72** 3150 (1994)
- [11] F. Ajzenberg-Selove, *Nucl.Phys. A* **523** 1-194 (1991), Data extracted from the ENSDF database for $A = 15$, revision of October 25, 2005, NNDC online service
- [12] J. H. Kelley, D. R. Tiley, H. R. Weller, C. M. Cheves, *Nucl.Phys. A* **564** 1 (1993), Data extracted from ENSDF database for $A = 17$, revision of October 25, 2005, NNDC online service
- [13] P. M. Endt, R. B. Firestone, *Nucl.Phys. A***633** 1 (1998), Data extracted from the ENSDF database for $A = 39$, revision of October 25, 2005, NNDC online service
- [14] A. Cameron, Balraj Singh, *Nuclear Data Sheets* **92** 429 (2001), Data extracted from the ENSDF database for $A = 41$, revision of October 25, 2005, NNDC online service
- [15] J. Tuli, *Nuclear Data Sheets* 1995, Data extracted from the ENSDF database for $A = 47$, revision of October 25, 2005, NNDC online service
- [16] T. W. Burrows, *Nuclear Data Sheets* 76(1995)191 A. Cameron, Balraj Singh, *Nuclear Data Sheets* **92** 429 (2001), Data extracted from the ENSDF database for $A = 49$, revision of October 25, 2005, NNDC online service
- [17] Huo Junde, *Nuclear Data Sheets* 64,723 (1991) Data, updated 2001, extracted from ENSDF database for $A = 55$, revision of October 25, 2005, NNDC online service
- [18] M. R. Bhat, *Nuclear Data Sheets* 85, 415 (1998), Data extracted from ENSDF database for $A = 57$, revision of October 25, 2005, NNDC online service
- [19] Y. V. Sergeenkov, Y. L. Khazov, T. W. Burrows, M. R. Bhat, *Nuclear Data Sheets* 72(1994)487, Data extracted from the ENSDF database for $A = 131$, revision of October 25, 2005, NNDC online service
- [20] S. Rab, *Nuclear Data Sheets* 75(1995)491, Data extracted from the ENSDF database for $A = 133$, revision of October 25, 2005, NNDC online service
- [21] M. J. Martin, *Nuclear Data Sheets* 70(1993)315, Data extracted from the ENSDF database for $A = 207$, revision of October 25, 2005, NNDC online service
- [22] M. J. Martin, *Nuclear Data Sheets* 63(1991)723, Data extracted from the ENSDF database for $A = 209$, revision of October 25, 2005, NNDC online service
- [23] C.H. Johnson, *Phys. Rev.* **C7**, 561 (1973); **C8**, 851 (1973).
- [24] D. W. Devins *et al.*, *Phys.Rev.* **C24** 1 (1981)
- [25] P. Doll, G.J. Wagner, K.T. Knipfle and G. Mairle, *Nucl.Phys. A***263** 210 (1976)
- [26] Y. Uozumi *et al.*, *Phys. Rev. C* **50**,263 (1994)
- [27] K. E. Rehm *et al.*, *Phys.Rev.Lett.* **80** 676 (1998)
- [28] S. Gales, G. M. Crawley, D. Weber, and B. Zwieglinski, *Phys. Rev. C* **18**,2475 (1978)
- [29] P. Grabmeyer *et al.*: *Jour. Phys. G* **18**, 1753 (1992)
- [30] H. Grawe, R. Schubart, K. H. Maier, D. Seweryniak, and the OSIRIS/NORDBALL Collaborations, *Phys. Scr.* T56(1995)71
- [31] G.W. Greenlees, G.J. Pyle, and Y.C. Tang, *Phys. Rev.* **171**, 1115 (1968).
- [32] P.E. Hodgson, *Rep. Prog. Phys.* **34** 765.
- [33] A. H. Hussein and H. S. Sherif, *Phys. Rev. C* **8**, 518 (1973).
- [34] V. I. Isakov, K. I. Erokhina, H. Mach, M. Sanchez-Vega, and B. Fogelberg, *Eur. Phys. J. A* **14**, 29 (2002).
- [35] V. I. Isakov, *Phys. Atom. Nuclei* **67**, 911 (2004).
- [36] H. Koura and M. Yamada, *Nucl. Phys. A***671**, 96 (2000).
- [37] A. M. Lane, *Phys. Rev. Lett.* **8**, 171 (1962); *Nucl. Phys.* **35**, 676 (1962).
- [38] E. Rost, *Phys. Lett. B* **26** 184 (1968)
- [39] J. Dudek, A. Majhofer, J. Skalski, T. Werner, S. Cwiok and W. Nazarewicz: *J. Phys. G* **5,10** 1359 (1979)
- [40] V.A. Chepurinov, *Yad.Fiz* 955 (1967)
- [41] J. Blomqvist and S. Wahlborn, *Ark. Fys.* 16 (1960) 543
- [42] A. Volya, in *3rd ANL/MSU/INT/JINA Theory Workshop*, Argonne National Laboratory, 4-7 April 2006 (World Scientific in press); *nucl-th/0605034*.
- [43] A. Volya and V. Zelevinsky, *Phys. Rev. Lett.* **94**, 052501 (2005); *Phys. Rev. C* 74, 064314 (2006).
- [44] <http://www.volya.net/ws>
- [45] S. Cwiok, J. Dudek, W. Nazarewicz, J. Skalski, T. Werner, *Comp.Phys.Comm.* **46**, 379 (1987)
- [46] K. Levenberg, *Quart.Appl.Math.* **2**, 164-168 (1944) and D. Marquardt, *SIAM J. Appl. Math.* **11**, 431-441 (1963)
- [47] I. Angeli: *Atomic Data and Nucl. Data Tables* **87**, 185 (2004)
- [48] M. Bender, G.F. Bertsch and P.-H. Heenen: *Phys.Rev C***73**, 034322 (2006)
- [49] A. Krasznahorkay *et al.*: *Phys.Rev.Lett* **82** 3216 (1999)
- [50] G. Audi, A.H. Wapstra and C. Thibault, *Nucl.Phys. A***729**, 337-676 (2003)
- [51] H. Sakaguchi, M. Nakamura, K. Hatanaka, T. Noro, F. Ohtani, H. Sakamoto, H. Ogawa, and S. Kobayashi, *Physics Letters B* **99**, 92 (1981).
- [52] T. Otsuka, R. Fujimoto, Y. Utsuno, B.A. Brown, M. Honma and T. Mitsuizaki: *Phys. Rev. Lett.* **87** 082502 (2001)
- [53] T. Otsuka, T. Suzuki, R. Fujimoto, H. Grawe, and Y. Akaishi, *Phys. Rev. Lett.* **95**, 232502 (2005).
- [54] G.A. Lalazissis, A.R. Farhan, M.M. Sharma, *Nucl. Phys. A* **628**, 221-254 (1998).
- [55] G.A. Lalazissis, D. Vretenar, P. Ring, M. Stoitsov, L.M. Robledo, *Phys. Rev. C* **60**, 014310 (1999) .
- [56] S. Peru, M. Girod, J.F. Berger, *Eur. Phys. J. A* **9**, 35-47 (2000).
- [57] R. Rodriguez-Guzman, J.L. Egido, L.M. Robledo, *Phys. Rev. C* 65, 024304 (2002).
- [58] J. Fridmann *et al.*: *Nature* 435,922 (2005)
- [59] J. Fridmann *et al.*,*Phys. Rev. C* **74**, 034313 (2006).
- [60] H. Scheit *et al.*, *Phys. Rev. Lett.* **77** (1996), 3967
- [61] T. Glasmacher *et al.*, *Phys. Lett. B* **395** (1997), 163
- [62] D. Guillemaud-Mueller, J.C. Jacmart, E. Kashy, A. Latimier, A.C. Mueller, F. Pougheon, A. Richard, E. YuA.G. Penionzhkevich, A.G. Arthuk, A.V. Belozyorow, S.M. Lukyanow, R. Anne, P. Bricault, C. Detraz, M. Lewitowicz and Y. Zhang: *Phys. Rev. C* **41**, 937 (1990)

- [63] M. Fauerbach, D.J. Morissey, W. Benenson, B.A. Brown, M. Hellstrm, J.H. Kelley, R.A. Kryger, R. Pfaff, C.F. Powell and B.M. Sherrill: Phys. Rev. **C 53**, 647 (1996)
- [64] J. Meng and P. Ring: Phys. Rev. Lett. **80**, 460 (1998)